Design of a Graphene Nitrene Two-Dimensional Catalyst Providing a Well-Defined Site Accommodating Up to Three Metals, with Application to N2 Reduction Electrocatalysis

KEYWORDS : Metal cluster catalysts(MCC), dope, nitrogen reduction, DFT

Li Li, and Lai Xu*

Institute of Functional Nano & Soft Materials (FUNSOM), Jiangsu Key Laboratory for Carbon-Based Functional Materials & Devices, Soochow University, Suzhou, 215123, China

Email: xulai15@suda.edu.cn; ORCID: orcid.org/0000-0003-2473-3359;

Computational Methods

Spin polarized density functional theory calculations were performed by using Vienna Ab Initio Simulation Package (VASP),[1] and the interaction of ions and electrons was described by the projector enhanced wave (PAW) method.[2] The exchange correlation between electrons is described by the generalized gradient approximation (GGA) in the form of a Perdew-Burke-Ernzerhof (PBE) function.[3] The energy cutoff for the plane-wave basis expansion was set to 450 eV. The Brillouin area of the inverted space was sampled by a method centered on the Gamma point. This scheme has a 4×4×1 k and 8×8×1 k point grid for the calculation of structural optimization and electronic properties respectively. The vacuum layer is set to 15 Å, the force on each atom is less than 0.05 eV $Å^{-1}$. We used the DFT-D3 method for vdW correction.[4] Bader charge calculation was applied to evaluate the charge transfer in different systems.[5]

The adsorption energy (Eads) of N_2 on the catalyst is defined as

$$E_{ads} = E_{N2\text{-}cat} - E_{N2} - E_{cat}, \quad (1)$$

where $E_{N2\text{-}cat}$, E_{N2} and E_{cat} respectively represents the total energy of N_2 adsorbed on the catalyst surface, energy of N_2 alone and energy of catalyst alone. Based on this definition, a negative value of E_{ads} shows that the adsorption is exothermic.

We used the computational hydrogen electrode (CHE) method[6] to calculate Gibbs free energy of the reaction for NRR. The free energy of the NRR step is defined as

$$\Delta G = \Delta E + \Delta E_{ZPE} - T\Delta S \quad (2)$$

where ΔE is the energy difference of DFT, ΔE_{ZPE} and TΔS are the change in zero energy and the change in entropy at 298.15 K, which is obtained by calculating the vibrational frequency. The catalytic activity is described by limiting potential ($U_{limiting}$), it is obtained using the equation: $U_{limiting} = -\Delta Gmax/e$.

Additional Figures

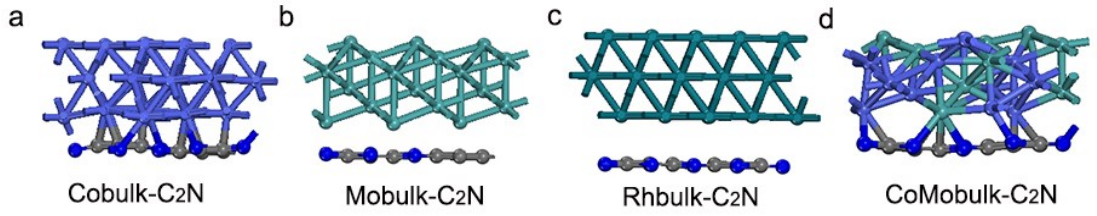

Figure S1. The optimized combination systems of metal bulk on the top of C_2N, (a-d) represent Cobulk-C_2N, Mobulk-C_2N, Rhbulk-C_2N and CoMobulk-C_2N.

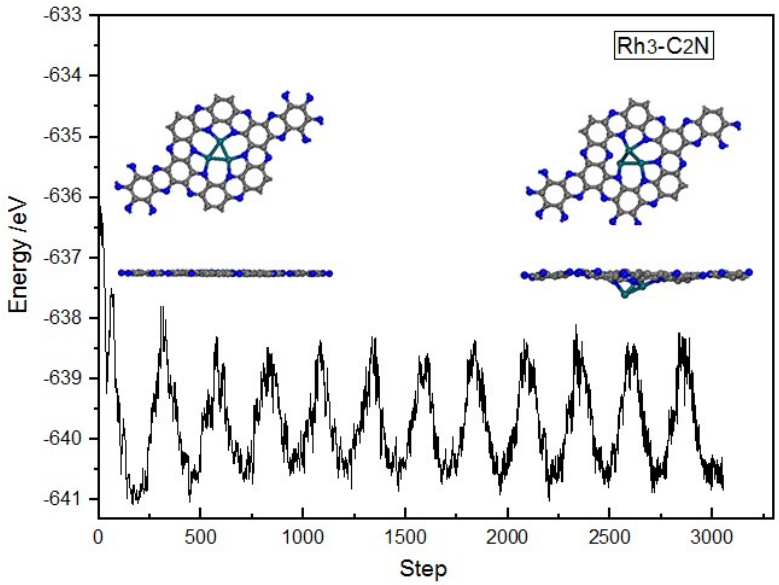

Figure S2. The ab initio molecular dynamics (AIMD) of Rh_3-C_2N. Total time is 9 ps, temperature is 300 K. the time step is 3 fs, the NVT ensemble was selected.

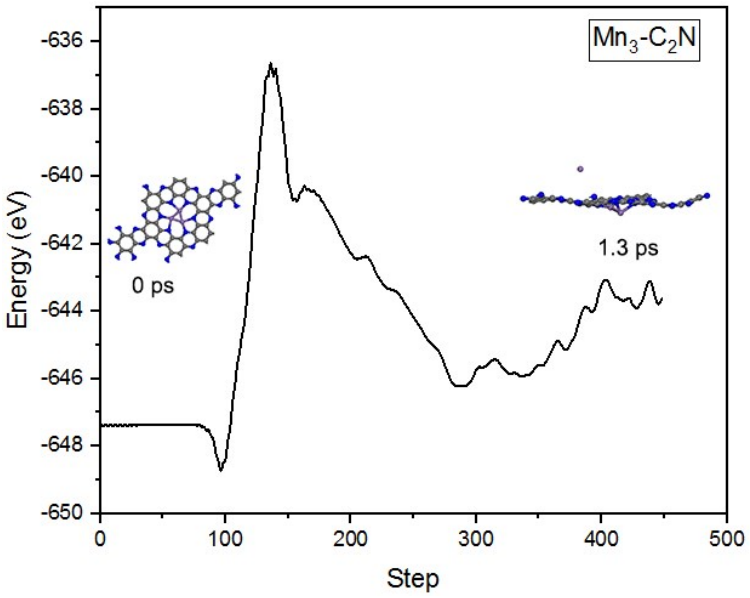

Figure S3. The ab initio molecular dynamics (AIMD) of Mn_3-C_2N. Total time is 1.3 ps, temperature is 300 K. TM cluster are destroyed, one metal atom stays away from C_2N substrate.

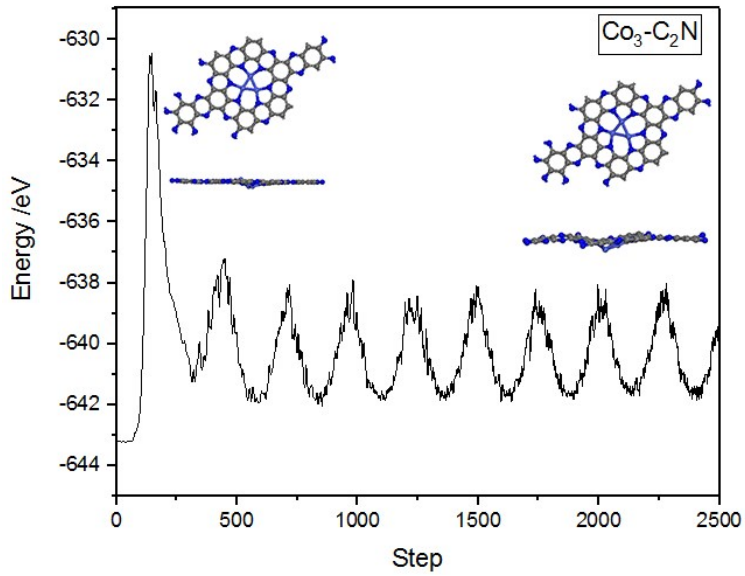

Figure S4. The ab initio molecular dynamics (AIMD) of Co_3-C_2N. Total time is 7.5ps. Temperature is 300 K.

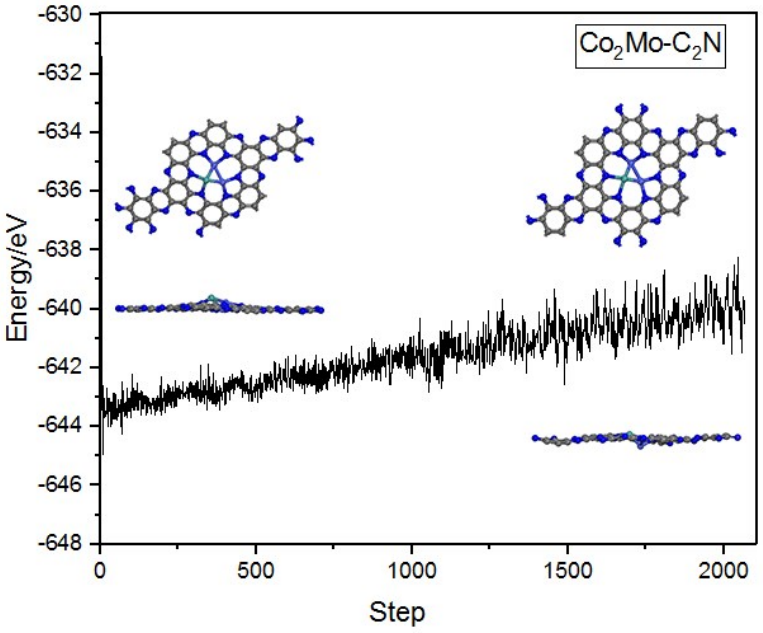

Figure S5. The ab initio molecular dynamics (AIMD) of Co_2Mo-C_2N. Total time is 6 ps. Temperature increases from 300 K to 1000 K.

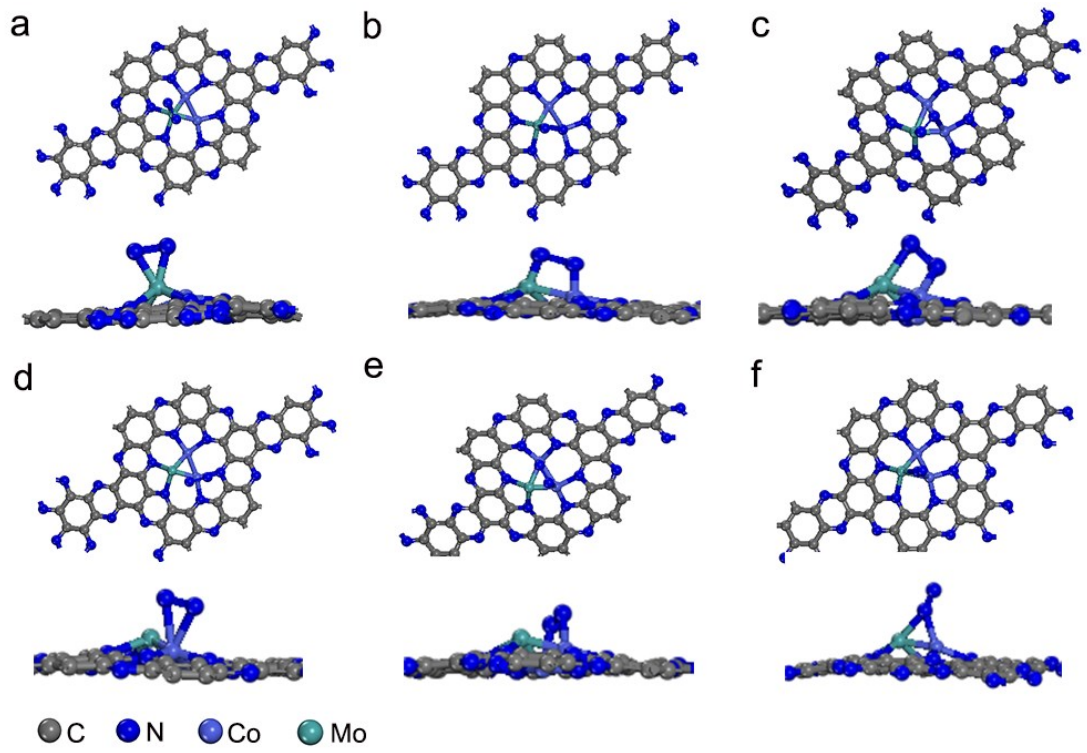

Figure S6. Possible adsorption configuration of N_2 molecules adsorbed on Co_2Mo-C_2N system.

We consider six adsorption modes of N_2. They are (a) N_2 parallel adsorption on Mo atoms; (b) N_2 parallel adsorption between Mo and Co atoms; (c) N_2 is bridged between Mo and bimetal Co, such as the position of the midline of the bottom edge of an isosceles triangle; (d) N_2 is adsorbed in parallel on Co atoms; (e) in parallel on two Co atoms; (f) vertical adsorption between Mo and Co atoms. It can be seen that N_2

molecules adsorbed on metal clusters are unlikely to dissociate directly into two isolated nitrogen atoms. The N_2 adsorption energy of these systems with different adsorption modes was calculated. The range of the adsorption energy is from -0.67 eV (a) to -1.22 eV (f) (see table S1 for details). Notably, after the optimization, the adsorption site of N_2 changes (Figure S6c), N_2 is adsorbed between Mo and Co metal atoms, and the structure is the same as Figure S6b. The adsorption energy of N_2 parallel (b), and vertical configurations between Mo and Co atoms (f) is larger, so we will focus on the reduction reaction process based on the correlation mechanism initiated by these two adsorption configurations.

Table S1. The adsorption energies of various N_2 configurations.

Configuration	a	b	c	d	e	f
Eads (eV)	-0.67	-1.17	-1.20	-0.91	-0.79	-1.22

Table S2. The $\Delta G(N_2H)$, $\Delta G(N_2)$ and $\Delta G(H)$ of single atom catalysts (SACs), double atom catalysts (DAC) and metal cluster catalysts (MCCs).

TM(1~3)-C_2N	$\Delta G(N_2)$/eV	$\Delta G(H)$/eV	$\Delta G(N_2H)$/eV
V_1	-0.59	-1.06	0.87
V_2	-1.54	-2.23	-0.11
V_3	-0.98	-0.25	0.60
Mn_1	-0.28	0.32	1.18
Mn_2	-0.72	-0.36	0.50
Mn_3	-3.69	-3.40	0.34
Fe_1	-0.07	0.72	0.71
Fe_2	-0.55	-0.52	0.30
Fe_3	-0.81	-1.02	0.71
Co_1	-0.84	0.27	1.30
Co_2	-0.87	-0.50	0.80
Co_3	-1.14	-1.10	0.18
Ni_1	-0.49	0.55	1.25
Ni_2	-0.71	-0.47	0.40
Ni_3	-1.30	-1.37	0.67
Cu_1	-0.59	0.61	1.82
Cu_2	-0.85	-1.02	0.74
Cu_3	-0.04	-2.18	0.52
Mo_1	-1.47	-1.24	0.43
Mo_2	No N_2 adsorption	/	/
Mo_3	-1.39	-0.70	0.63
Ru_1	-0.81	-0.49	0.89
Ru_2	-0.48	-0.22	1.25
Ru_3	-1.40	-0.63	1.06
Rh_1	-0.49	0.22	1.34
Rh_2	-0.50	-0.45	1.16
Rh_3	-5.73	-4.96	0.31

Pt_1	No N_2 adsorption	/	/
Pt_2	-1.35	-2.05	1.34
Pt_3	-1.35	-0.44	1.07
CoMo	-1.00	-0.39	0.60
Co_2Mo	-1.01	-0.83	0.45
$CoMo_2$	-0.73	-0.19	0.68

Table S3. The $\Delta G(N_2H)$ of TMbulk-C_2N，TMbulk=CoMo bulk, Rh bulk.

TMbulk-C_2N	Rh bulk	CoMo bulk
$\Delta G(N_2H)$/eV	1.10	1.11

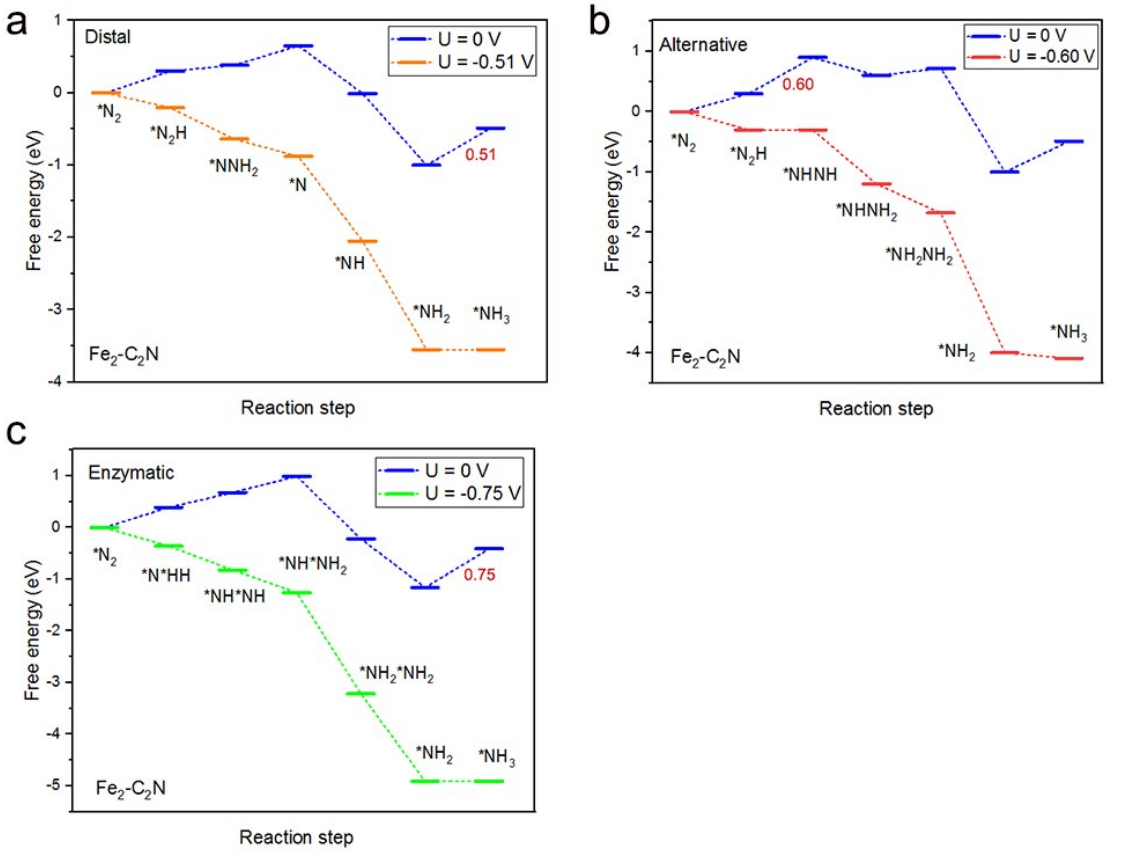

Figure S7. Gibbs free energy diagrams for NRR on Fe_2-C_2N along distal pathway, alternating pathway and enzymatic pathway.

We considered the competitive reaction and $\Delta G(N_2H)$ of the corresponding single-diatomic and diatomic systems. The $\Delta G(N_2)$ of the Fe_1-C_2N system is very small ($\Delta G(N_2)$ = -0.07 eV), indicating that its adsorption capacity for N_2 is very poor, and the value of $\Delta G(N_2H)$ is large (0.71 eV). The catalytic activity of Fe_1-C_2N system is low. Although Fe_3-C_2N has a better adsorption effect for N_2, its ability to adsorb H is stronger, so the hydrogen evolution reaction tends to occur. The value of ΔG (N_2H) is 0.71 eV, indicating that the NRR catalytic ability is weak, Fe_2-C_2N system has a strong ability to adsorb N_2 ($\Delta G(N_2)$ = -0.55 eV) better than H ($\Delta G(H)$ = -0.52 eV), and the first step reaction is easy to occur ($\Delta G(N_2H)$ = 0.30 eV), so it is a

promising diatomic catalyst (Table S2). Three reaction pathways of the system are calculated (Figure S7), of which the limiting potential of the distal pathways is -0.51 eV versus RHE(Figure S7a), which is the optimal path for the reduction reaction.

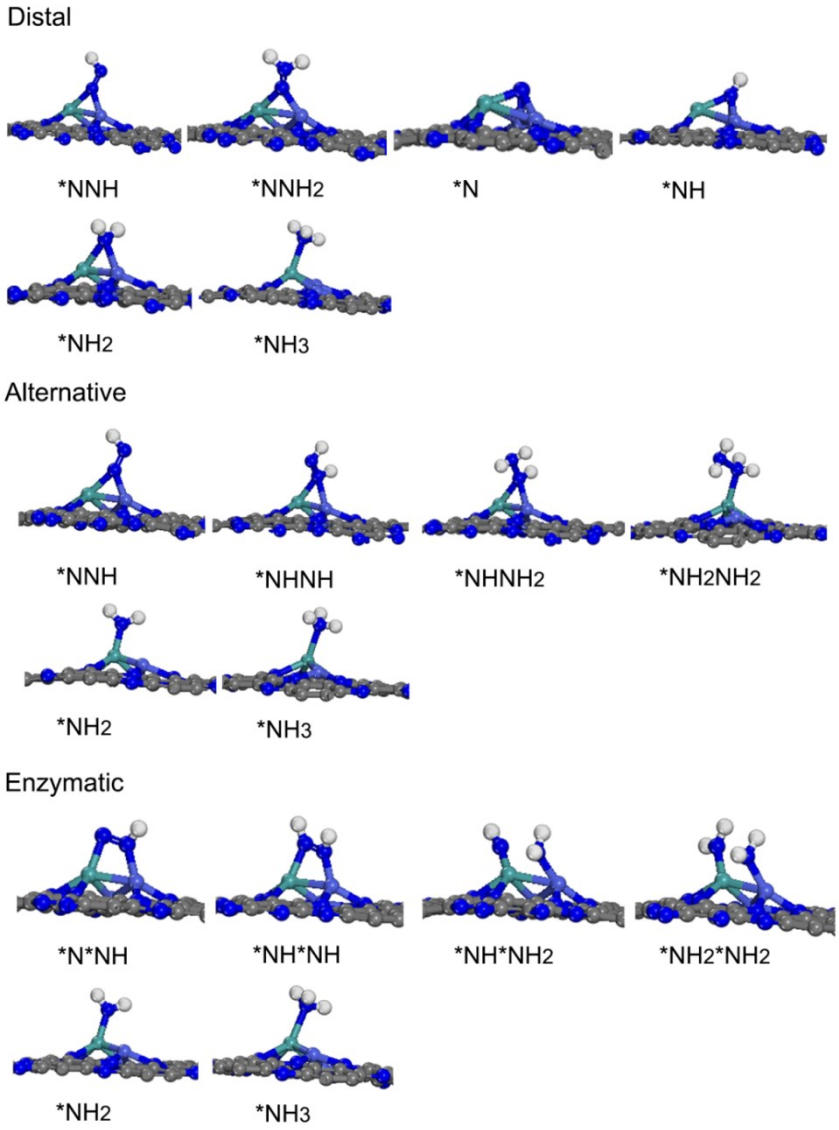

Figure S8. Intermediate structures of Co_2Mo-C_2N system in the three pathways.

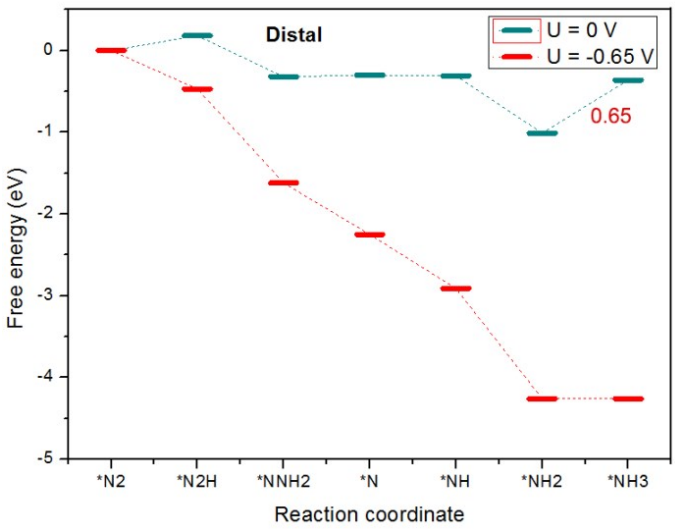

Figure S9. Gibbs free energy diagrams for NRR on Co_3-C_2N along distal pathway.

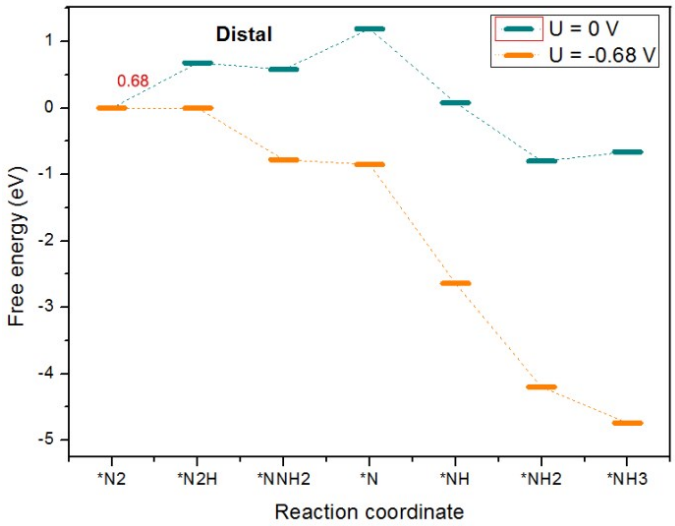

Figure S10. Gibbs free energy diagrams for NRR on $CoMo_2$-C_2N along distal pathway.

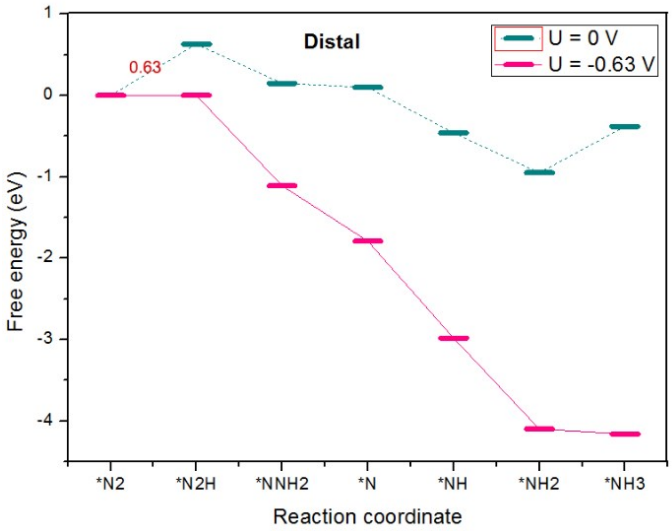

Figure S11. Gibbs free energy diagrams for NRR on Mo_3-C_2N along distal pathway.

In addition, we also compared the NRR reaction pathway of the Co_3-C_2N, Mo_3-C_2N, $CoMo_2$-C_2N and CoMo bulk-C_2N system, such as the distal pathway. Specifically, the maximum Gibbs free energy increase of N_2 catalyzed by the Co cluster catalyst is 0.65 eV, and the RDS step is NH_2 reduction to NH_3. In one step, the ΔGmax of the Mo cluster catalyst is 0.63 eV, and the RDS step is the first step (formation of N_2H). For $CoMo_2$-C_2N system, limiting potential (U_L) is -0.68 V versus RHE is required to form N_2H. For CoMo-C_2N and CoMobulk-C_2N systems, ΔG（N_2H）are 0.60 eV and 1.11 eV separately (Table S2, S3), which are larger than that of Co_2Mo-C_2N. Therefore, we found that a cluster catalyst with one Co atom and two Mo atoms has the best catalytic effect (Figure S9, S10, S11, Table S3).

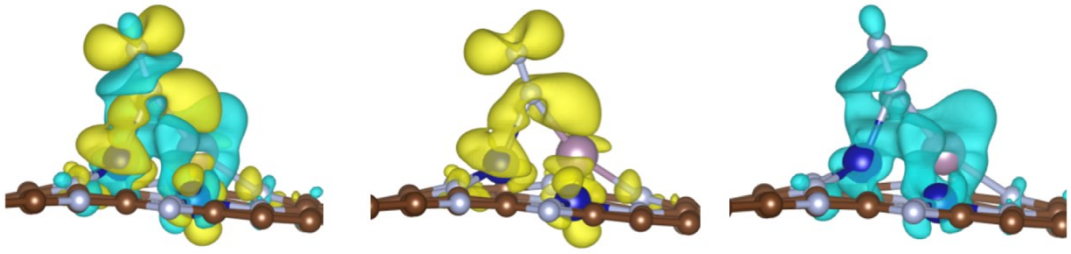

Figure S12. Differential charge of N_2 adsorbed on Co_2Mo-C_2N, yellow represents obtaining charges, blue represents losing charges.

Figure S12 is a differential charge diagram for the Co_2Mo-C_2N structure. Charge flow analysis shows that the charge transfer between the metals and adsorbed N_2 is bidirectional, the empty d orbitals of the metals accept the lone pair electrons from N_2, the occupied d orbitals of the metal provides electrons to the π* orbitals of N_2, and promotes the breaking of the NN triple bond. The combination of the metal's empty d orbit and occupied d orbit plays a key role in the adsorption of N_2.

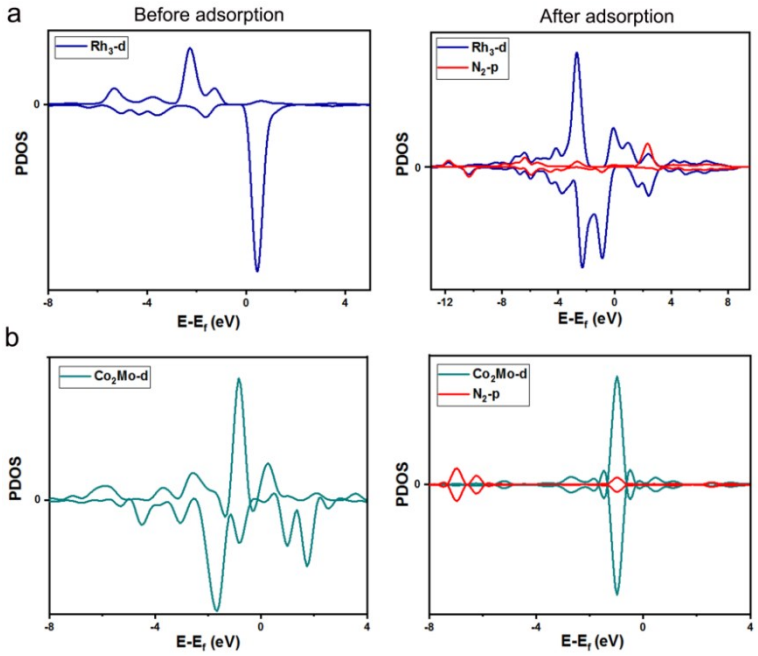

Figure S13. (a, b) PDOS before and after adsorption of N_2 on Rh_3-C_2N and Co_2Mo-C_2N. The Fermi level was set to be zero.

Figure S13a, S13b show a wide overlap between the d orbitals of the metal atoms (Rh_3, Co_2Mo) and the sp orbital of N_2, for after adsorption of N_2 on Rh_3-C_2N, there was a clear overlap on a peak near -4~0 eV, for after adsorption of N_2 on Co_2Mo-C_2N, there was a clear overlap on a peak near -1 eV, indicating that there were a strong hybridization between the TM orbitals and N_2 orbitals in this state.

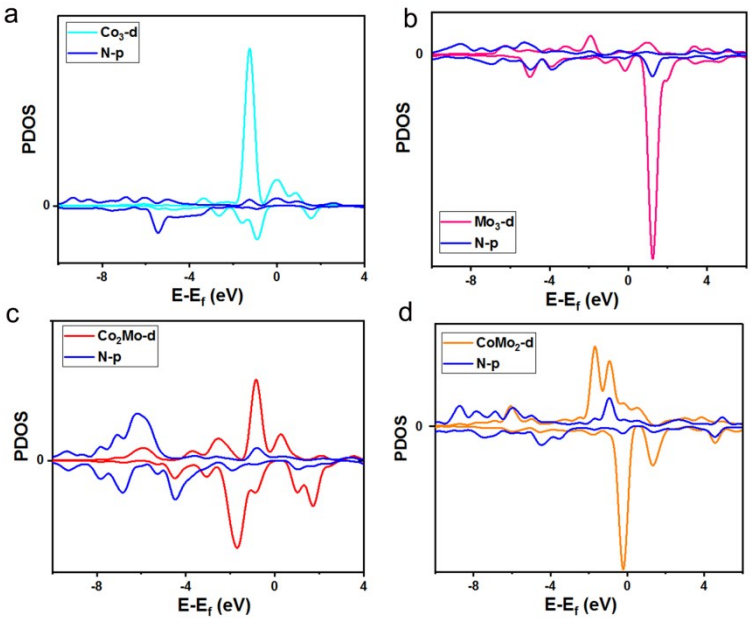

Figure S14. (a, b, c, d) Projected density of states (PDOS) of Co_3-C_2N, Mo_3-C_2N, Co_2Mo-C_2N and $CoMo_2$-C_2N.

The partial density of states (PDOS) of MCCs indicates that the electronic interaction mainly exists between TM_3-d and N (from C_2N)-2p orbitals, The valence electrons of metal clusters saturate the semi-full orbitals of N in C_2N (Figure S14a, S14b, S14c, S14d).

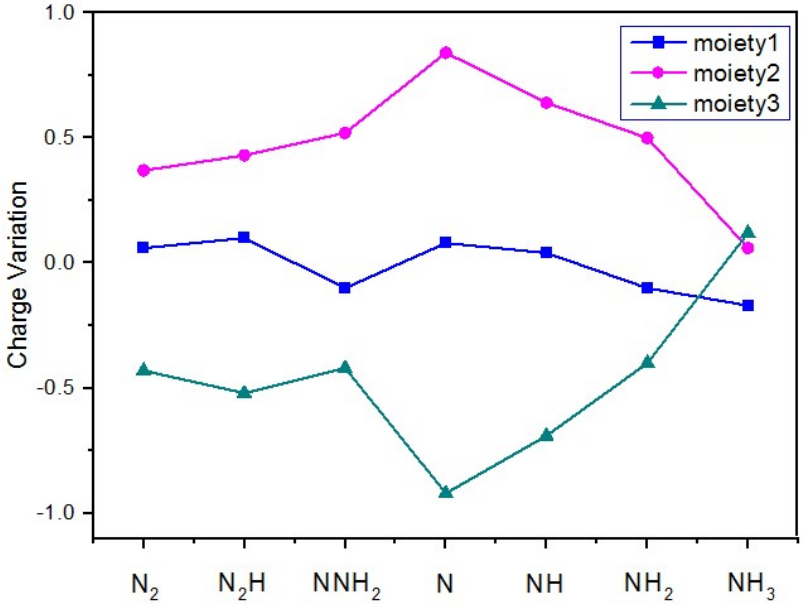

Figure S15. Charge variation of the three moieties for Co_2Mo-C_2N. Moiety 1 represents the CN substrate, Moiety 2 represents the 6 nitrogen atoms (Co_2MoN_6) adjacent to the metal, and Moiety 3 represents the adsorption species (NxHy).

In order to better illustrate the catalytic properties, the Bader charge as shown in Figure S13 was calculated and analyzed. Group 1 represents the CN substrate, group 2 represents the 6 nitrogen atoms (Co_2MoN_6) adjacent to the metal, and group 3 represents the adsorption species (NxHy). The nitrogen adsorption approach is vertical adsorption. The pathway to generate NH_3 is a distal mechanism. In the first step of adsorption of N_2, the CN and Co_2MoN_6 parts lost 0.06 and 0.37 electrons, respectively. During the subsequent reduction step, significant charge fluctuations occurred in both parts. After the first NH_3 was formed, the CN substrate lost 0.08 electrons, Co_2MoN_6 lost 0.84 electrons, and *N gained 0.92 electrons. When the second NH_3 was formed, NH_3 transferred 0.12 electrons back to the CN monolayer. In the entire reaction pathway, the charge on the CN substrate hardly changes. Co_2MoN_6 acts as the activation center, transferring most of the electrons to the adsorbed species, thereby activating the intermediate and continuing the subsequent reactions.

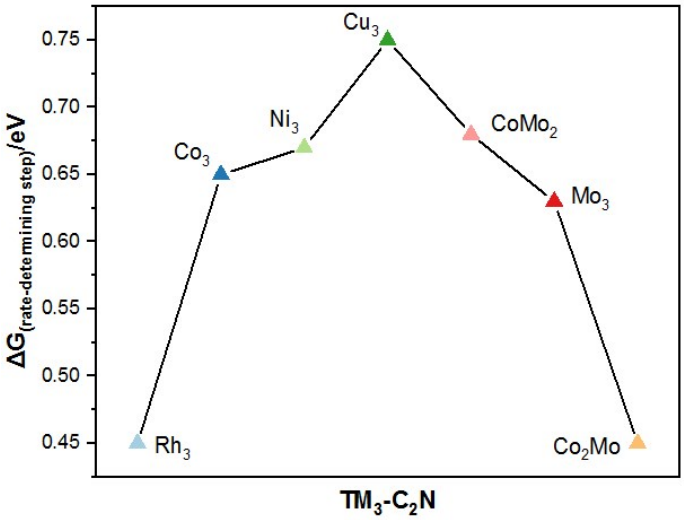

Figure S16. Relationship diagram between the activity and free energy of model catalysts.

References:

1. Kresse, G.; Furthmüller, J., Efficiency of ab-initio total energy calculations for metals and semiconductors using a plane-wave basis set. *Computational Materials Science* **1996,** *6* (1), 15-50.

2. Kresse, G.; Joubert, D., From ultrasoft pseudopotentials to the projector augmented-wave method. *Physical Review B* **1999,** *59* (3), 1758.

3. Perdew, J. P.; Burke, K.; Ernzerhof, M., Generalized gradient approximation made simple. *Physical Review Letters* **1996,** *77* (18), 3865.

4. Grimme, S.; Antony, J.; Ehrlich, S.; Krieg, H., A consistent and accurate ab initio parametrization of density functional dispersion correction (DFT-D) for the 94 elements H-Pu. *The Journal of Chemical Physics* **2010,** *132* (15), 154104.

5. Henkelman, G.; Arnaldsson, A.; Jónsson, H., A fast and robust algorithm for Bader decomposition of charge density. *Computational Materials Science* **2006,** *36* (3), 354-360.

6. Norskov, J. K.; Rossmeisl, J.; Logadottir, A.; Lindqvist, L.; Kitchin, J. R.; Bligaard, T.; Jonsson, H., Origin of the overpotential for oxygen reduction at a fuel-cell cathode. *J. Phys. Chem. B* **2004,** *108* (46), 17886-17892.